PHYSICAL REVIEW C

NUCLEAR PHYSICS

THIRD SERIES, VOLUME 30, NUMBER 2 AUGUST 1984

Proton radiative capture into closed-shell and closed-shell-plus-one-proton nuclei

S. L. Blatt, H. J. Hausman, L. G. Arnold, R. G. Seyler, R. N. Boyd, T. R. Donoghue, and P. Koncz*
Department of Physics, The Ohio State University, Columbus, Ohio 43210

M. A. Kovash†
Massachusetts Institute of Technology, Cambridge, Massachusetts 02139

A. D. Bacher and C. C. Foster
Department of Physics, Indiana University, Bloomington, Indiana 47401
(Received 30 March 1984)

Radiative proton capture reactions into nuclei with closed subshells and into the neighboring nuclei with one additional proton produce gamma-ray spectra with remarkably similar major features. Detailed measurements of ^{11}B(p,γ)^{12}C and ^{12}C(p,γ)^{13}N, described here, reveal additional striking similarities. A generalized direct-semidirect picture of the reaction is presented, from which quantitative relationships between such capture reaction pairs may be derived, including comparisons of angular distributions, analyzing powers, and cross-section ratios over a wide range of bombarding energies. The data are in good agreement with the theoretical predictions.

I. INTRODUCTION

Since our discovery[1] of strong proton radiative capture transitions to high-lying states in ^{12}C and ^{28}Si, several approaches have been explored[2–4] in attempts to understand various aspects of the observations. In our original interpretation of the data, we suggested that the most strongly populated final states were of one-particle–one-hole character, with the "stretched" configurations (4^-, $\sim$19 MeV in ^{12}C; 6^-, $\sim$14 MeV in ^{28}Si) dominating the observed γ-ray spectra. Arnold[2] and Tsai and Londergan[3] showed that such an assumption leads to a reasonable description of the spectra, and, if a direct-capture mechanism is assumed, the magnitudes of the observed cross sections for $E_p > 40$ MeV are also reproduced satisfactorily. Below this energy, a resonant mechanism is present.[5–8] In a simple single-particle picture,[5] the resonance arises from 1p-1h configurations with the particle at a $2\hbar\omega$ excitation, while the final state after γ decay has the particle at $1\hbar\omega$. This led to the description of the resonance as a "second harmonic giant resonance." Recently, Anghinolfi *et al.*[9] have reported the observation of giant resonances built on many of the excited states of ^{12}C, including those in the 19-MeV region; the Brookhaven-University of Washington collaboration[10] has seen similar results in ^{27}Al(p,γ)^{28}Si. These new observations, added to the earlier results indicating an inability to explain the γ_{19} cross section in the 24–40 MeV region with a simple direct capture mechanism,[7,8] reinforce the earlier giant resonance interpretation for this transition. No microscopic calculation has yet been done to explain this resonance in detail, but a phenomenological direct-semidirect calculation[8] indicates that such a description should be possible.

In studying other features of our early observations, Arnold[2] also noted that the γ-ray spectrum of ^{11}B(p,γ)^{12}C had major features remarkably similar to those of ^{12}C(p,γ)^{13}N. In fact, in the simple independent-particle picture, the spectrum of a (p,γ) reaction into a closed-subshell-plus-one-proton nucleus would be expected to resemble that for capture into the neighboring closed-subshell nucleus, except that the simple single-particle configurations seen as final states in the former case are spread out by the particle-hole coupling in the latter. In Figs. 1 and 2 we show spectra from ^{11}B(p,γ)^{12}C and ^{12}C(p,γ)^{13}N at $E_p = 28.5$ MeV. One notes that the dominant feature in the latter is the capture transition $\gamma_{2,3}$, which is believed[11] to go predominantly into the $d_{5/2}$ third excited state, while in the former, the strongest transitions are to the cluster of states near 19 MeV in ^{12}C which are of $(d_{5/2}, p_{3/2}^{-1})$ character. The γ-ray energies of these corresponding transitions in the two nuclei are very nearly identical.

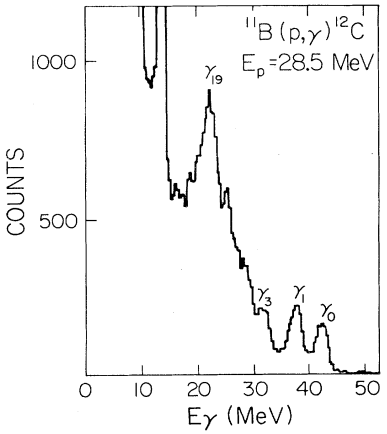

FIG. 1. The spectrum of gamma rays from the $^{11}B(p,\gamma)^{12}C$ reaction taken at a detector angle of 60°. All gamma rays in the spectrum above an energy of approximately 16 MeV are capture-gamma-ray transitions to excited states of ^{12}C. The peak labeled γ_0 at 42 MeV is the transition to the ground state of ^{12}C; the peak γ_{19} is from transitions to a group of states including the 4^- stretched 1p-1h states at 19.4 MeV.

After the initial observation, two additional neighboring pairs of nuclei were also studied, to see whether similar results would be obtained. The reactions investigated were (a) $^{27}Al(p,\gamma)^{28}Si$ and $^{28}Si(p,\gamma)^{29}P$, and (b) $^{15}N(p,\gamma)^{16}O$ and $^{16}O(p,\gamma)^{17}F$. As we reported earlier,[5,12] the neighboring pairs in both cases show the same simple relationship, with the energies of major capture gamma rays being remarkably similar despite large differences in ground-state Q values and excitation energies.

In the present paper, we report detailed measurements of the $^{11}B(p,\gamma)^{12}C/^{12}C(p,\gamma)^{13}N$ reaction pair. We also present details of a generalized direct-semidirect picture of such reactions. Predictions of the picture are compared

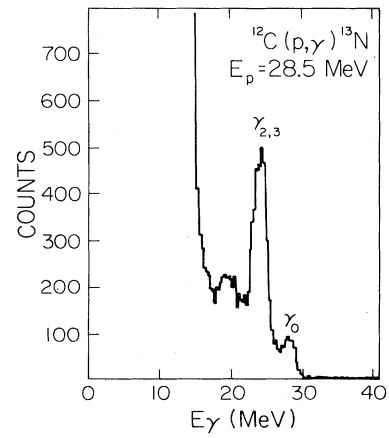

FIG. 2. The spectrum of gamma rays from the $^{12}C(p,\gamma)^{13}N$ reaction taken at a detector angle of 60°. The peak labeled γ_0 at 28 MeV is the transition to the ground state of ^{13}N; the $\gamma_{2,3}$ peak is primarily the transition to the $\frac{5}{2}^+$ single particle state in ^{13}N at an excitation energy of 3.55 MeV.

to the observations, not only for the "γ_{19}" transition in ^{12}C and $^{12}C(p,\gamma_3)^{13}N$, but also for the transition pair $^{11}B(p,\gamma_2)^{12}O(2^+$, 4.44 MeV) and $^{12}C(p,\gamma_0)^{13}N(\frac{1}{2}^-$, ground state). In this latter pair, the ^{12}C 2^+ state is considered as a $p_{1/2}$ proton coupled to a $p_{3/2}$ hole, while the ^{13}N ground state has a simple $p_{1/2}$ proton configuration.

In the next section, we describe the experimental work on these two reactions, including both angular distribution and analyzing power measurements and a determination of the energy dependence of the capture cross sections. Section III describes the direct-semidirect picture in its general form; comparisons with the data for the specific cases we have measured are contained in Sec. IV.

II. EXPERIMENTAL PROCEDURE AND RESULTS

Self-supporting targets of enriched ^{11}B and ^{12}C were bombarded by polarized and unpolarized proton beams at the Indiana University Cyclotron Facility (IUCF). The boron targets were enriched to 97.1% ^{11}B and the ^{12}C targets were enriched to 99.9%. A number of different targets were utilized in the measurements and generally had thicknesses in the range 20—35 mg/cm^2.

An anticoincidence-shielded large-crystal (25.4×30.48 cm) NaI(Tl) detector and associated electronics, designed and built at The Ohio State University, was used to detect gamma rays in the energy range 20—100 MeV from capture reactions. Details of the physical structure and performance for this detector are described in Ref. 13. The detector system utilizes time-of-flight information to reject neutron-induced events; the time resolution was 2.3 ns and provided good discrimination between gamma-ray and neutron events at all bombarding energies used in these studies. At beam currents from 10 to 50 nA, total counting rates in the NaI(Tl) crystal were as high as 2×10^5 per second. Pileup rejection circuitry was incorporated to the NaI(Tl) channel to eliminate virtually all spectral distortion from this source; linear pulse shortening reduced potential pileup to less than 10%, and an auxiliary logic system easily handled the residual events. A photomultiplier gain-stabilization system,[14] capable of operating at rates well over 3×10^5 pulse/s, maintained gain stability to within ±1% over runs extending from 4 to 8 h in duration. The detector was positioned some 1 m from the target and subtended a solid angle of 9.37 msr for some runs and 13.3 msr for others. The detector resolution at $E_\gamma=45$ MeV was about 3.8% FWHM.

A spectrum of gamma rays from the $^{11}B(p,\gamma)^{12}C$ reaction taken at a proton energy of 28.5 MeV is shown in Fig. 1. Gamma rays corresponding to decays to the ground and first excited states of ^{12}C are observed well resolved from one another. In addition to the strong decay to excited states at ~19 MeV in ^{12}C, containing the stretched $(d_{5/2},p_{3/2}^{-1})$ 4^- state(s) in ^{12}C, one observes decays to a number of other presumably particle-hole negative parity states in ^{12}C at excitation energies between 9.6 and 18 MeV. Using the measured line shape for this detector, we were able to separate the spectra into their various components and determine absolute cross sections to within ±20% for most of the states. The fitting routine established that the unresolved cluster of states in the

19 MeV excitation region was well described by three states at approximately 18.4, 19.6, and 20.6 MeV. These states apparently correspond to the $T=0$ and $T=1$, $J^{\pi}=4^{-}$ stretched particle-hole states, seen also in pion[15] and electron[16] scattering, and one or more 3^{-} particle-hole states.

A spectrum of gamma rays from the $^{12}C(p,\gamma)^{13}N$ reaction at a proton energy of 28.5 MeV is shown in Fig. 2. The dominant decay in this spectrum is to the well-known $\frac{5}{2}^{+}$ single-particle state in ^{13}N at an excitation energy of 3.55 MeV. Weaker decays to the ground state of ^{13}N and to unresolved higher-lying states can also be seen in the spectrum.

The energy dependence of the 60° differential cross section of $^{11}B(p,\gamma)$ capture to the 2^{+} first excited state of ^{12}C (capturing into a $p_{1/2}$ configuration) and the companion $^{12}C(p,\gamma_0)^{13}N$ cross section (also $p_{1/2}$) are shown in Fig. 3(a). $^{11}B(p,\gamma)$ captures to the cluster of states at an excitation energy of 19 MeV in ^{12}C are shown in Fig. 3(b). As can be seen from the figure, this latter reaction, populating $d_{5/2}$ configurations, has a resonance behavior with a maximum cross section of 4 μb/sr occurring at a bombarding energy of $\sim$30 MeV. Details and interpretations of this resonance are described in Refs. 5–7. The energy dependence of the differential cross section of gamma-ray decays to the $\frac{5}{2}^{+}$, 3.55 MeV, excited state in ^{13}N is also shown in Fig. 3(b). This cross section has a maximum value of 4.4 μb/sr at a bombarding energy of $\sim$29 MeV.

Analyzing-power measurements were performed at a proton bombarding energy of 28.5 MeV near the peaks of the resonant cross sections in both ^{12}C and ^{13}N. Beam currents varied from 8 to 20 nA and the beam polarization, measured before and after each run, ranged, in different runs, from 0.61 to 0.67. The results of the angular distributions of the analyzing power and cross sections are shown in Figs. 4 and 5. Cross section angular depen-

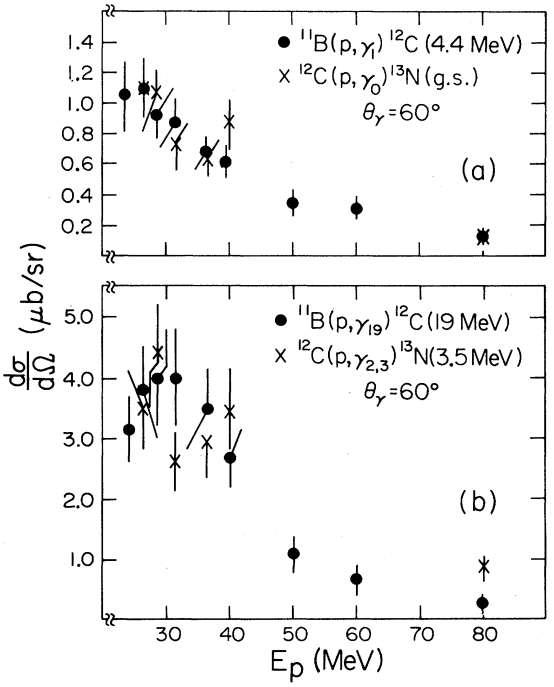

FIG. 3. The energy dependence of the cross section for (a) proton capture into the $p_{1/2}$ orbital in ^{12}C and ^{13}N, and (b) proton capture into the $d_{5/2}$ orbital plotted as a function of laboratory proton energy.

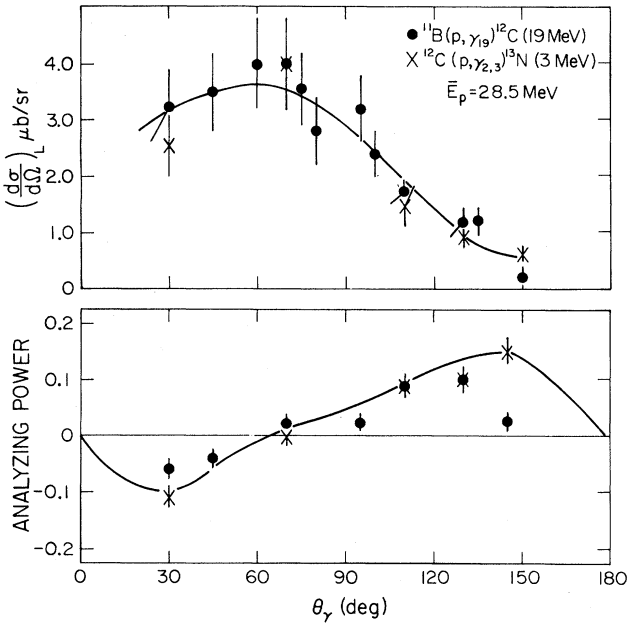

FIG. 4. Gamma-ray angular distribution shapes and analyzing powers for proton capture into the $d_{5/2}$ orbital in the $^{11}B(p,\gamma)^{12}C$ and $^{12}C(p,\gamma)^{13}N$ reactions. The indicated cross section scale is appropriate for $^{11}B(p,\gamma)$, while the $^{12}C(p,\gamma)$ data have been normalized by matching, at 70°, for a direct comparison of shapes. The solid curves are least-squares Legendre polynominal and associated Legendre polynominal fits.

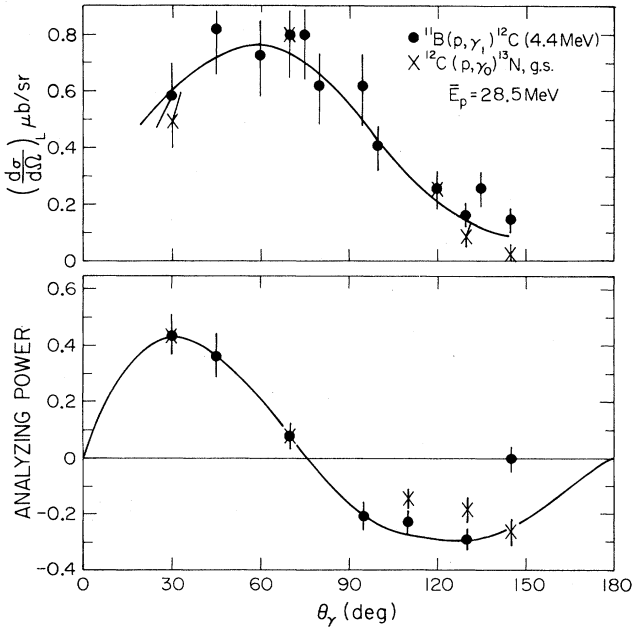

FIG. 5. Same as Fig. 4, except that the proton is captured into the $p_{1/2}$ orbital.

dences are essentially identical between pairs. The angular dependence of the analyzing powers for the $^{11}B(p,\gamma)^{12}C^*$(19 MeV) and the $^{12}C(p,\gamma)^{13}N^*$(3.55 MeV) reactions are also strikingly similar, while the angular dependence of $^{11}B(p,\gamma)^{12}C^*$(4.43 MeV) and $^{12}C(p,\gamma)^{13}N$(g.s.), while different from the previously mentioned pair, again closely resemble each other.

III. THEORY

In this section we develop the methodology for comparing a nucleon radiative capture transition into a closed-shell nucleus with a related transition into an adjacent closed-shell-plus-one-nucleon nucleus. We begin with a review of the direct capture or spectator model. This is motivated by a problem encountered in our initial attempt to assess the limitations of the model and its extension to include semidirect processes in the initial state. Specifically, there is a prevalent view in previous work[4,8,17] that it is necessary or natural to assume that the final state populated in direct plus semidirect capture consists of a nucleon coupled to the target ground state. As an alternative to the customary formulation of the direct-semidirect model, we identify assumptions which define a class of radiative capture models that includes a shell model picture of direct and semidirect capture as special cases. These assumptions are the following: (1), the initial and final states in the capture process can be represented by states constructed from orthogonal one-nucleon configurations; (2), the electromagnetic transition operator can be represented as a sum of one-nucleon operators. The first assumption is the standard truncation which defines the shell model description of nuclear bound and continuum states.[18] It differs from the customary formulation based on a nucleon coupled to an unspecified target state by imposing the standard truncation on the target states. The second assumption is implicit in conventional analyses and both assumptions are accepted practice in calculations. The net result of formalizing them is a surveyable model system from which the limitations of the direct-semidirect model, as routinely used, can be assessed. In particular, the orthogonality properties of the assumed states result in strong constraints on the capture process. The comparison procedure above is then developed for this direct-semidirect picture and its predictions are summarized.

We denote the transition amplitude for the radiative capture process by

$$M=\langle\psi_f\,|\,H^\lambda\,|\,\psi_i\rangle = \langle J_f M_f T_f T_{f3}\,|\,H^\lambda\,|\,J_i M_i s m_s T_i T_{i3} t t_3\rangle\ , \tag{1}$$

where the initial state ψ_i and the final state ψ_f are eigenstates of a nuclear Hamiltonian H with energies E_i and E_f, respectively, and H^λ is the electromagnetic interaction Hamiltonian which acts as a transition operator for creation of a photon with energy $E_\gamma=E_i-E_f$ and helicity λ. The initial state is specified by the angular momentum and isospin quantum numbers of the target nucleus ground state (J_i,M_i,T_i,T_{i3}) and the quantum numbers of the incident nucleon $(s=\frac{1}{2},m_s,t=\frac{1}{2},t_3)$; the final state is specified by its total angular momentum and isospin quantum numbers (J_f,M_f,T_f,T_{f3}). The differential cross section and analyzing power for the transition are given by

$$\sigma=\hat{s}^{-2}\hat{J}_i^{-2}\,\mathrm{Tr}(MM^\dagger)\ , \tag{2}$$

$$\sigma A_y=\hat{s}^{-2}\hat{J}_i^{-2}\,\mathrm{Tr}(M\sigma_y M^\dagger)\ , \tag{3}$$

where $\hat{x}^2=2x+1$ and Tr represents the sum over M_i, m_s, M_f, and λ.

The essential features of the direct capture model and its limitations are concisely described by employing the projection operator formalism. Let P be a projection operator which projects from the space of the nuclear Hamiltonian that part which corresponds to a nucleon coupled to the target ground state; let Q be the complement of P. With these definitions, M can be written

$$M=\langle P\psi_f\,|\,H^\lambda\,|\,P\psi_i\rangle+\langle P\psi_f\,|\,H^\lambda\,|\,Q\psi_i\rangle + \langle Q\psi_f\,|\,H^\lambda\,|\,P\psi_i\rangle+\langle Q\psi_f\,|\,H^\lambda\,|\,Q\psi_i\rangle\ . \tag{4}$$

The first term on the right-hand side is the direct capture amplitude, the second and third terms are called the initial and final state semidirect amplitudes, while the last is nondirect or compound. The direct capture model corresponds to retaining the first term,

$$M_d=\langle P\psi_f\,|\,H^\lambda\,|\,P\psi_i\rangle\ , \tag{5}$$

and ignoring the others. Neglect of the amplitudes which depend on $Q\psi_i$ is justified, at least in lowest order, in that the initial state ψ_i evolves from an asymptotic state where $Q\psi_i=0$. The radiative capture transition is initiated by a nucleon incident on a particular state of the target; therefore, the state ψ_i, however complicated, must obey boundary conditions appropriate to this designated entrance channel. In contrast, there is no constraint which requires ψ_f to evolve, even in lowest order, to an asymptotic state with $Q\psi_f=0$. There is no designated exit channel in the radiative capture process. In general, ψ_f will have components for each channel with an amplitude for a given channel determined from spectroscopic considerations for that channel. In the case of $P\psi_f$, it follows from the definition of the projection operator P that $P\psi_f$ is proportional to the spectroscopic amplitude for a nucleon coupled to the ground state of the target. Analogous results hold for any channel in the Q subspace that is specifically isolated and considered. Since there are many final states, particularly at high excitation energies, which have small spectroscopic factors for a nucleon coupled to the target ground state and, hence, a possible large spectroscopic factor for some channel in the Q subspace, neglect of the amplitudes in Eq. (4) which depend on the $Q\psi_f$ cannot be justified in the same way as the dependence on $Q\psi_i$. Under these circumstances, the direct capture model is expected to be a viable description of transitions to isolated low lying final states that are known to have the ground state of the target as the dominant parent. It is not clear, however, that the model is applicable to transitions to high lying states where the spectroscopy is less certain. This problem carries over to the phenomenological direct-semidirect model where the first two terms in Eq.

(4) are retained,

$$M_{dsd}=\langle P\psi_f \mid H^\lambda \mid P\psi_i\rangle+\langle P\psi_f \mid H^\lambda \mid Q\psi_i\rangle \ , \tag{6}$$

with $Q\psi_i$ approximated by a single state which represents a nucleon coupled to a coherent one particle-one hole excitation of the target ground state.

Our model, which includes direct and semidirect capture, is developed from the two general assumptions stated earlier: (1), the initial state ψ_i and final state ψ_f can be represented by states constructed from orthogonal one-nucleon configurations; (2), H^λ can be represented as a sum of one-nucleon operators. (1) is the primary assumption of the shell model approach to nuclear reactions.[18] It is a natural nuclear structure assumption for a class of nucleon radiative capture models, although its limitations are numerous and difficult to circumvent. Assumption (2) is also applicable to a class of radiative capture models of which direct capture is the simplest member. Its limitations can hardly be ignored since it is known that H^λ contains two-body operators, due to the exchange of charged mesons between the nucleons, that provide an important correction to the photoabsorption sum rule. The extent to which violations of these assumptions are important in spectroscopic applications of radiative capture is a question that is beyond the scope of this paper.

The relevance of these assumptions stems from the following arguments: First, we note by way of comparison that the target nucleon configurations in the initial and final states of $\langle P\psi_f \mid H^\lambda \mid P\psi_i\rangle$ are identical. It then follows from the orthogonality of the P and Q subspaces that the initial and final states of both $\langle P\psi_f \mid H^\lambda \mid Q\psi_i\rangle$ and $\langle Q\psi_f \mid H^\lambda \mid P\psi_i\rangle$ must differ by at least one target nucleon configuration. Second, we note that a sum of one-body operators is capable of changing the configuration of only one particle in a many-particle state constructed from orthogonal one-body configurations; transitions between two such states are forbidden if the states differ by two or more one-body configurations. Thus, $\langle P\psi_f \mid H^\lambda \mid Q\psi_i\rangle=0$ unless the projectile nucleon configurations in $Q\psi_i$ and $P\psi_f$ are identical, and $\langle Q\psi_f \mid H^\lambda \mid P\psi_i\rangle=0$ unless the projectile nucleon configurations in $Q\psi_f$ and $P\psi_i$ are identical. In other words, the components of $Q\psi_i$ and $Q\psi_f$ which contribute to the semidirect amplitudes must be one-particle—one-hole excitations of the target ground state with the projectile nucleon configuration playing the role of spectator. Recall that the target ground state is a spectator in the direct amplitude. There are no comparable constraints on the nondirect amplitude $\langle Q\psi_f \mid H^\lambda \mid Q\psi_i\rangle$. We now write the semidirect amplitudes in Eq. (4) as

$$\begin{aligned}\langle P\psi_f \mid H^\lambda \mid Q\psi_i\rangle &= \langle P\psi_f \mid H^\lambda \mid q(P)\psi_i\rangle \\ &= \langle P\psi_f \mid H^\lambda A_i(P) \mid P\psi_i\rangle \ , \end{aligned} \tag{7a}$$

$$\begin{aligned}\langle Q\psi_f \mid H^\lambda \mid P\psi_i\rangle &= \langle q(P)\psi_i \mid H^\lambda \mid P\psi_i\rangle \\ &= \langle P\psi_f \mid A_f(P)^\dagger H^\lambda \mid P\psi_i\rangle \ , \end{aligned} \tag{7b}$$

where $q(P)$ is a projection operator which projects from the space of the nuclear Hamiltonian that part which corresponds to all configurations consisting of a nucleon coupled to one-particle—one-hole excitations of the target ground state. While $q(P)$ is a subspace of Q, it need not be identified with physical excited states of the target; to the contrary, it is known that the strength of a given particle-hole excitation may be distributed over a number of target excited states. Thus, we make a distinction for the semidirect amplitudes between the customary partition of the Q subspace in terms of physical excited states of the target and that used above where the Q subspace is partitioned according to the particle-hole excitations of the target ground state. The operator $A(P)$ in Eqs. (7) is defined by $q(P)\psi_i=A(P)P\psi_i$ and may be written

$$A(P)=[E-q(P)\mathscr{H}q(P)]^{-1}q(P)\mathscr{H}P \ , \tag{8}$$

where

$$\mathscr{H}=H+Hr(E-rHr)^{-1}rH \tag{9}$$

with $Q=q(P)+r$. The transition amplitude is now written

$$M=\langle P\psi_f \mid H^\lambda_{\rm eff}(P) \mid P\psi_i\rangle+\langle Q\psi_f \mid H^\lambda \mid Q\psi_i\rangle \ , \tag{10}$$

where

$$H^\lambda_{\rm eff}(P)=H^\lambda+H^\lambda A_i(P)+A_f(P)^\dagger H^\lambda \tag{11}$$

is an effective transition operator that includes both direct and semidirect capture mechanisms. The second term in Eq. (10) is the nondirect amplitude unaltered from Eq. (4). If this term is neglected, the transition amplitude reduces to a form analogous to the direct-semidirect amplitude originally introduced by Brown[19] for electric dipole capture in the long wavelength limit. Since the first term in Eq. (10) includes all multipolarities without approximation, we take

$$M_{dsd}=\langle P\psi_f \mid H^\lambda_{\rm eff}(P) \mid P\psi_i\rangle \tag{12}$$

as the definition of the direct-semidirect model with approximate forms of the model deriving from approximations to the effective transition operator in Eq. (11). For example, it is customary to neglect the final state semidirect operator, $A_f(P)^\dagger H^\lambda$, since it is much smaller than the direct and initial state semidirect operators, H^λ and $H^\lambda A_i(P)$, in typical applications of the model. The single state coherent particle-hole approximation to Eqs. (8) and (9) then leads directly to the phenomenological direct-semidirect model. The direct capture model is recovered by neglecting both of the semidirect operators in Eq. (11).

A remarkable consequence of the present formulation, which is in marked contrast to the customary specification of the direct capture model,[4,8] is the absence of any assumptions on the parentage of ψ_f. In the direct capture model, those components of the final state whose parentage derives from the projectile and target in the entrance channel are populated. Assumptions about the specific structure of the final state are subsumed by this selection rule.[2] The selection rule is preserved in the direct-semidirect model since the semidirect amplitudes populate the same components of the final state as the direct amplitude, albeit via an intermediary of one-particle—one-hole excitations of the target ground state. The selection rule is preserved because the allowed intermediate excitations retain the target ground state parentage of the en-

trance channel. We regard this rule as the most important signature of a direct-semidirect radiative capture process. While it has been obtained here for nucleon radiative capture, the assumptions on which it is based are general enough to warrant considering its use for radiative capture initiated by other light ions and in heavy ion collisions. The direct-semidirect selection rule is violated by nondirect mechanisms that contribute to the amplitude $\langle Q\psi_f \mid H^\lambda \mid Q\psi_i \rangle$.

We now consider the nondirect amplitude $\langle Q\psi_f \mid H^\lambda \mid Q\psi_i \rangle$ that is neglected in the direct-semidirect model. Let $Q=P'+Q'$, where P' is a projection operator which projects that part of the space of H which corresponds to the first excited state of the target and $Q'=1-P-P'$ is the remaining complement. With this definition, the nondirect amplitude takes the same form as Eq. (4),

$$\begin{aligned}\langle Q\psi_f \mid H^\lambda \mid Q\psi_i \rangle &= \langle P'\psi_f \mid H^\lambda \mid P'\psi_i \rangle + \langle P'\psi_f \mid H^\lambda \mid Q'\psi_i \rangle \\ &\quad + \langle Q'\psi_f \mid H^\lambda \mid P'\psi_i \rangle + \langle Q'\psi_f \mid H^\lambda \mid Q'\psi_i \rangle \ . \end{aligned} \tag{13}$$

The terms in Eq. (13) may be classified "direct," "semidirect," and "nondirect" in the same way as the amplitudes in Eq. (4), and the preceding arguments about the semidirect amplitudes of Eq. (4) may be applied to the semidirect terms in Eq. (13). The result is that Eq. (13) may be written

$$\begin{aligned}\langle Q\psi_f \mid H^\lambda \mid Q\psi_i \rangle &= \langle P'\psi_f \mid H^\lambda_{\rm eff}(P') \mid P'\psi_i \rangle \\ &\quad + \langle Q'\psi_f \mid H^\lambda \mid Q'\psi_i \rangle \ , \end{aligned} \tag{14}$$

where $H^\lambda_{\rm eff}(P')$ has the same form as $H^\lambda_{\rm eff}(P)$ in Eq. (11) with $A(P')$ defined in the same manner as $A(P)$. This procedure can be repeated for each excited state of the target and its isobaric analog until the Q space is exhausted, and thus leads to the following hierarchy for M:

$$\begin{aligned}M &= \langle P\psi_f \mid H^\lambda_{\rm eff}(P) \mid P\psi_i \rangle + \langle P'\psi_f \mid H^\lambda_{\rm eff}(P') \mid P'\psi_i \rangle \\ &\quad + \cdots + \langle X\psi_f \mid H^\lambda_{\rm eff}(X) \mid X\psi_i \rangle + \cdots \ , \end{aligned} \tag{15}$$

where $P+P'+\cdots+X+\cdots=1$ and $H^\lambda_{\rm eff}(X)$ has the same form as $H^\lambda_{\rm eff}(P)$ in Eq. (11) with $A(X)$ defined in the same manner as $A(P)$. The net result of this procedure is a sequence of amplitudes, one for each state of the target and its analog, that have the common form of a direct-semidirect amplitude. Each amplitude in the sequence contains a direct term and a pair of semidirect terms which involve one-particle—one-hole excitations of the target or analog state. To the extent that the single state coherent particle-hole approximation is applicable to the semidirect terms, Eq. (15) contains a formal confirmation of the Brink hypothesis.[20] In addition, Eq. (15) exhibits a generalization of the direct-semidirect capture selection rule given above for the target ground state to a selection rule that is applicable to each state of the target and its isobaric analog: A nucleon radiative capture transition to a final state component whose parentage is target state X must be initiated from components of the initial state whose parentages are target state X for the direct amplitude and one-particle—one-hole excitations of target state X for the semidirect amplitudes. The population of these initial state components from the projectile and target in the entrance channel is a separate problem governed by the dynamics of the nuclear Hamiltonian H. Once populated, however, the path to the final state is uniquely determined.

Components of the initial state whose parentages are excited states of the target may be obtained by making the customary partition of the Q subspace in terms of these physical target states and solving the resulting coupled equations. The solutions may be written formally as

$$\mid X\psi\rangle = (E - XH_{\rm eff}X)^{-1}XH_{\rm eff}P \mid P\psi\rangle \ , \tag{16}$$

where $H_{\rm eff}=H+HY(E-YHY)^{-1}YH$ with $P+X+Y=1$. It follows that the importance of a given component is governed by the strength of nuclear inelastic transitions between the two channels. Low lying collective excited states of the target have strong coupling to the target ground state via such transitions, and are therefore expected to be important contributors to the nondirect amplitude $\langle Q\psi_f \mid H^\lambda \mid Q\psi_i \rangle$ in radiative capture. In this regard, to the extent that a given collective excited state of the target is important, one-particle—one-hole excitations of this collective state need to be considered.

One of the more important collective nuclear excitations, both generally and in the specific context of nucleon radiative capture,[21] is the isobaric analog of the target ground state. If this excitation is retained and all others neglected, Eq. (15) reduces to

$$M = \langle P\psi_f \mid H^\lambda_{\rm eff}(P) \mid P\psi_i \rangle + \langle A\psi_f \mid H^\lambda_{\rm eff}(A) \mid A\psi_i \rangle \ , \tag{17}$$

where A is the projection operator for the analog. There are two situations where the analog component of Eq. (17) is absent: neutron radiative capture for target nuclei with $T_3 \geq 0$, and proton radiative capture for target nuclei with $T_3 \leq 0$. For all other situations, both pairs of amplitudes are present. However, the nuclear interactions responsible for the transition to the analog are also reponsible for the electromagnetic charge-exchange currents which lead to two body operators H^λ; as such, retention of the analog component of Eq. (17), without considering two-body operators in H^λ, represents an incomplete approach to the role of charge-exchange interactions in radiative capture. We neglect analog components of Eq. (17) as being beyond the scope of the present paper.

In the preceding discussion, we have developed a surveyable model of the radiative capture process and have shown that the primary limitation of the direct-semidirect model [Eq. (12)] is the presence of collective excitations of the target ground state which contribute to the nondirect amplitude $\langle Q\psi_f \mid H^\lambda \mid Q\psi_i \rangle$. The coherent electric dipole excitation of *all* target states is included in this model in a natural way through the semidirect terms included in Eqs. (12) and (15). The importance of this excitation stems from the dominance of electric dipole radiative capture. Thus, the validity of the direct-semidirect model is limited by the presence of other collective excitations of the target ground state which are strongly coupled to it via nuclear

inelastic transitions.

We now develop the methodology for comparing a nucleon radiative capture transition into a closed-shell nucleus with a related transition into an adjacent closed-shell-plus-one nucleon nucleus. Since $\langle P\psi_f \mid$ in Eq. (12) is proportional to $(C^2S)^{1/2}$, where C^2S is the conventional spectroscopic factor, the transition amplitude M_{dsd} is reducible to the form

$$M_{dsd}=\sum_j (C^2S)^{1/2}\langle J_iM_ijm \mid J_fM_f\rangle M_{dsd}(j) , \tag{18}$$

where

$$M_{dsd}(j)=\langle jm \mid h^{\lambda}_{dsd} \mid sm_s\rangle \tag{19}$$

denotes the transition amplitude for capture of the incident nucleon to a final state single particle orbital of angular momentum j, $|J_i-J_f| \le j \le J_i+J_f$, and parity $\pi=\pi_i\pi_f$. On substituting Eq. (18) into Eqs. (2) and (3), the expressions for the cross section and analyzing power become

$$\sigma=\frac{J_f^2}{\hat{s}^2\hat{J}_i^2}\sum_j \hat{j}^{-2}(C^2S)^{1/2}\,\mathrm{Tr}[M_{dsd}(j)M_{dsd}(j)^{\dagger}] , \tag{20}$$

$$\sigma A_y=\frac{J_f^2}{\hat{s}^2\hat{J}_i^2}\sum_j \hat{j}^{-2}(C^2S)^{1/2}\,\mathrm{Tr}[M_{dsd}(j)\sigma_yM_{dsd}(j)^{\dagger}] , \tag{21}$$

with Tr now representing a sum over m_s, m, and λ. In Eqs. (20) and (21), the nuclear structure information associated with the transition resides in the angular momentum and spectroscopic factors. The transition amplitudes $M_{dsd}(j)$ contain the reaction kinematics and dynamics with a residual of structure dependence coming from the average nuclear field of the target ground state and the average nuclear field of the coherent one-particle—one-hole excitation of the target ground state. Since these average fields are expected to vary slowly with mass number and energy, the nuclear structure dependence of $M_{dsd}(j)$ is a negligible effect in a comparison of transitions for adjacent nuclei; by negligible, we mean significantly smaller than the nominal 20% uncertainty in spectroscopic factors. Thus, if two dynamically equivalent transitions are compared under appropriately matched kinematic conditions, the amplitudes $M_{dsd}(j)$ for the two transitions should be equal.

The starting point for comparing a radiative capture transition into a closed-shell nucleus with a related transition for an adjacent nucleus with an additional nucleon is the latter. Since $J_i=0$ for the target in the transition to a nucleus with a closed-shell-plus nucleon, this transition proceeds via capture to a unique final state orbital with $j^{\pi}=J_f^{\pi}$. We use $j_f=j=J_f$ to distinguish this j and J_f from the closed-shell case and write the cross section and analyzing power for the closed-shell-plus-one transition, including isospin $t_f=T_f$, as

$$\sigma(0,j_f,j_f)=\frac{1}{\hat{s}^2}C^2S(0,j_f,j_f,t_f)\,\mathrm{Tr}[M_{dsd}(j_f)M_{dsd}(j_f)^{\dagger}] , \tag{22a}$$

$$A_y(0,j_f,j_f)=\frac{\mathrm{Tr}[M_{dsd}(j_f)\sigma_yM_{dsd}(j_f)^{\dagger}]}{\mathrm{Tr}[M_{dsd}(j_f)M_{dsd}(j_f)^{\dagger}]} . \tag{22b}$$

Comparison of this transition with a transition to a state in the adjacent closed-shell nucleus is meaningful only if the closed-shell transition is dominated by a single j value with $j=j_f$. Thus, we write the cross section and analyzing power for the closed-shell transition as

$$\sigma(J_i,j_f,J_f)=\frac{\hat{J}_f^2}{\hat{J}_i^2\hat{j}_f^2\hat{s}^2}C^2S(J_i,j_f,J_f,T_f)\,\mathrm{Tr}[M_{dsd}(j_f)M_{dsd}(j_f)^{\dagger}] , \tag{23a}$$

$$A_y(J_i,j_f,J_f)=\frac{\mathrm{Tr}[M_{dsd}(j_f)\sigma_yM_{dsd}(j_f)^{\dagger}]}{\mathrm{Tr}[M_{dsd}(j_f)M_{dsd}(j_f)^{\dagger}]} . \tag{23b}$$

If two transitions are compared under similar, if not identical, kinematic conditions, the $M_{dsd}(J_f)$ in Eqs. (22) and (23) may be treated as equal; that is,

$$M_{dsd}(j_f)\mid_{J_ij_fJ_f}=M_{dsd}(j_f)\mid_{0j_fj_f} , \tag{24}$$

for reasons noted above. This leads to the following predictions: (a), the cross section angular distributions for the two transitions have the same shape; (b), their analyzing powers are equal,

$$A_y(J_i,j_f,J_f)=A_y(0,j_f,j_f) ; \tag{25}$$

(c), their cross section magnitudes are related by

$$\frac{\sigma(J_i,j_f,J_f)}{\sigma(0,j_f,j_f)}=\frac{\hat{J}_f^2}{\hat{J}_i^2\hat{j}_f^2}\frac{C^2S(J_i,j_f,J_f,T_f)}{C^2S(0,j_f,j_f,t_f)} . \tag{26}$$

These predictions are idealized in that it may not be possible to achieve appropriately matched kinematics for a given pair of transitions: their kinematic limitations are discussed in the next section where the predictions are compared with experiment.

IV. ANALYSIS

In this section we apply the results from the preceding section to the data for the ^{11}B(p,γ)^{12}C and ^{12}C(p,γ)^{13}N cases. We consider two cases: (i) is a comparison of

^{11}B(p,γ_{19})^{12}C(4$^-$ at 19 MeV) with ^{12}C(p,γ_3)^{13}N($\frac{5}{2}^+$ at 3.55 MeV); (ii) is a comparison of ^{11}B(p,γ)^{12}C(2$^+$ at 4.4 MeV) with ^{12}C(p,γ_0)^{13}N(g.s.). The initial as well as the final states for each of these reaction pairs are expected to be comparable in the manner described previously. In the extreme shell model picture, for case (i) the $T=0$ and $T=1$ 4$^-$ states near 19 MeV in ^{12}C consist of $1d_{5/2}1p_{3/2}^{-1}$ excitation of the 0$^+$ ground state of ^{12}C. The ground state of ^{11}B has a $1p_{3/2}$ hole, while the $\frac{5}{2}^+$ state at 3 MeV in ^{13}N has a $1d_{5/2}$ particle configuration. In the same spirit, for case (ii) the 2$^+$ state of ^{12}C is a $1p_{1/2}1p_{3/2}^{-1}$ excitation of the ^{12}C ground state 0$^+$ and the ^{13}N ground state configuration is a $p_{1/2}$ particle coupled to the ^{12}C ground state. Thus case (ii) transitions are structurally similar in that each involves capture into the $1p_{1/2}$ state.

The kinematics for the two case (i) reactions are sufficiently similar that when the two reactions are compared at the same proton energy the gamma energies are nearly equal. The kinematics for the reaction data shown in Fig. 4 are as follows. For ^{11}B(p,γ_{19}), E_p(c.m.) is 26.1 MeV and E_γ is 22.7 MeV; for ^{12}C(p,γ)^{13}N($\frac{5}{2}^+$), E_p(c.m.) is 26.3 MeV and E_γ is 21.9 MeV. As a result of the similar kinematics the entrance channel distortions for the two reactions should be similar with the result that the transition amplitudes $M_{dsd}(j)$ should be approximately equal if the reaction mechanisms for the two reactions are the same. If the $M_{dsd}(j)$ are equal then the analyzing powers and the shapes of the angular distributions for the two reactions will be equal as described in Sec. III. Figure 4 shows a comparison of the angular distributions and analyzing powers for ^{11}B(p,γ_{19})^{12}C and ^{12}C(p,γ_3)^{13}N($\frac{5}{2}^+$) at $E_p^{(lab)}$ equal to 28.5 MeV. It is seen that the shapes of the cross section angular distributions are approximately equal and the same is true for the analyzing power distributions, as expected if the $M_{dsd}(j)$ are approximately equal.

The observed ratio R of the total cross sections at a particular energy for the two case (i) reactions will involve contributions in the form of Eq. (26) from each unresolved final state (J_f^π,T) of ^{12}C, i.e.,

$$R=\sum_{J_f,T} R(J_f^\pi,T) . \tag{27}$$

From Eq. (26),

$$R(4^-,T)=\left[\frac{9}{48}\right]\frac{S(\frac{3}{2},\frac{5}{2},4^-,T)}{S(0,\frac{5}{2},\frac{5}{2}^+,\frac{1}{2})} ,$$

and the numerical factors for $J_f^\pi=1^-$, 2$^-$, and 3$^-$ are $\frac{3}{48}$, $\frac{5}{48}$, and $\frac{7}{48}$, respectively. If all possible $d_{5/2}p_{3/2}^{-1}$ states, i.e., $J_f^\pi=4^-$, 3$^-$, 2$^-$, and 1$^-$ for both $T=0$ and 1 were degenerate at 19 MeV excitation and if each had the same spectroscopic factor S, the sum in Eq. (27) would reduce to

$$R=\frac{S}{S(0,\frac{5}{2},\frac{5}{2}^+,\frac{1}{2})} ,$$

i.e., the multiplicative angular momentum and isospin factor would be unity. The observed γ_{19} transition is believed to include contributions at least from states having (J_f^π,T) values of (4$^-$,1), (4$^-$,0), and (3$^-$,1), which are known to be in that energy region. If these three states had the same spectroscopic factor S, Eq. (27) for the cross section ratio R to be compared with experiment would become

$$R=\left[\frac{25}{48}\right]\frac{S}{S(0,\frac{5}{2},\frac{5}{2}^+,\frac{1}{2})} . \tag{28}$$

Turning to the spectroscopic factors, the recent experimental results of Peterson and Hamill[22] for the $\frac{5}{2}^+$ state of ^{13}N suggest $S(0,\frac{5}{2},\frac{5}{2}^+,\frac{1}{2})=0.5$. Having no experimental S values for the high-lying negative parity states in ^{12}C, we note that the spectroscopic factor for the (3$^-$,1) state has been calculated by two groups. Donnelly and Walker[23] obtain the value 0.984 and Hanna *et al.*[24] report the value 0.862. The result that these values are close to unity coupled with the fact that the 4$^-$ states of ^{12}C are stretched configuration particle hole states (unique parentage), which suggests that their S values would be at least as large as that of the (3$^-$,1) state, supports our adopting a single spectroscopic factor $S=0.9$ for these three states. Inserting the spectroscopic factors into Eq. (34) the cross section ratio for case (i) becomes

$$R=\left[\frac{25}{48}\right]\frac{(0.9)}{(0.5)}=0.94 . \tag{29}$$

Figure 3(b) shows the ^{11}B(p,γ_{19})^{12}C and ^{12}C(p,$\gamma_{2,3}$)^{13}N cross sections at $\theta_\gamma=60°$ over the range of proton c.m. energies from 24 to 80 MeV. It is seen that the two cross sections are approximately equal over the entire energy range. Thus the experimental cross section ratio is about unity, in good agreement with the Eq. (29) result [based on similar $M_{dsd}(j)$] over the whole energy range covered, which includes both resonant and nonresonant capture. We note that the case (i) reactions are ideal for purposes of comparison since the entrance and exit channel kinematics are so similar for the two reactions.

A similar comparison of the case (ii) transitions [^{11}B(p,γ_1)^{12}C(2$^+$) and ^{12}C(p,γ_0)^{13}N(g.s.)] reveals, as can be seen in Fig. 5, that they also have approximately equal cross section angular distributions and equal analyzing power distributions. It should be noted that while the cross section angular distributions are similar to the corresponding case (i) distributions, the analyzing powers for case (ii) are approximately inverted compared to case (i). This might be expected since the case (i) reactions correspond to capture into a $j=l+\frac{1}{2}$ orbital whereas case (ii) involves capture in a $j=l-\frac{1}{2}$ orbital. The analyzing power for the ^{11}B(p,γ_0)^{12}C transition (capture to a $p_{3/2}$ orbital) is compatible with this picture.[25]

While a comparison of case (ii) transitions at the same bombarding energy gives approximately the same E_p(c.m.) values, the E_γ values are quite different. For example, the kinematics for the data in Fig. 5, where $E_p=28.5$ MeV, has $E_\gamma=37.9$ MeV for ^{11}B(p,γ_1) and $E_\gamma=28.4$ MeV for ^{12}C(p,γ_0), a difference of order 30%. Of course, for higher E_p, the relative difference between the E_γ values is smaller. Nevertheless for the case (ii) comparison, it is impossible to have approximately equal

energetics for the two transitions for any of the E_p values available. A comparison of the reactions at the same E_p minimizes differences in entrance channel distortion for the two reactions. If a single multipole dominates the exit channels the angular distributions (of cross section and analyzing power) are independent of the exit channel (gamma) kinematics. Thus the angular distributions will be the same in spite of exit channel kinematic differences in the $M_{dsd}(j)$, provided that the reactions are dominated by a single multipole. The data for the case (ii) comparison shown in Fig. 5 are consistent with the dominance of a single multipole and otherwise equal values of the $M_{dsd}(j)$. At higher energies, where more than one multipole might contribute, the differences in the $M_{dsd}(j)$ due to the difference in γ kinematics would be proportionately smaller.

The ratio of the total cross sections for the case (ii) reactions should, according to Eq. (26), be

$$\frac{\sigma(\frac{3}{2},\frac{1}{2},2)}{\sigma(0,\frac{1}{2},\frac{1}{2})}=\left[\frac{5}{8}\right]\left[\frac{1}{2}\right]\frac{S(\frac{3}{2},\frac{1}{2},2,0)}{S(0,\frac{1}{2},\frac{1}{2},\frac{1}{2})}=0.92\ .$$

The spectroscopic factor $S(\frac{3}{2},\frac{2}{2},2,0)=1.41$ for the 4.4 MeV 2^+ state of ^{12}C is taken from Adelberger *et al.*[26] who discuss the variety of values available, while the factor $S(0,\frac{1}{2},\frac{1}{2},\frac{1}{2})=0.48$ for the g.s. of ^{13}N is taken from Peterson and Hamill.[22] For this case where experimental spectroscopic factors are available we note that they agree well with theoretical values of Cohen and Kurath.[27] Figure 3(a) shows the cross sections at $\theta_\gamma=60°$ for the case (ii) reactions over the proton c.m. energies from 26 to 80 MeV. It is seen that the two cross sections are approximately equal over the entire energy range. This result is in good agreement with the above estimate which is based on the assumption that the $M_{dsd}(j)$ of the two reactions are equal. This assumption is open to question since the exit channel (γ) kinematics, which are included in $M_{dsd}(j)$, are, as discussed above, quite different for the two case (ii) reactions. An alternative which would minimize differences in gamma kinematics, would be to compare the reactions at the same gamma energies. Such a comparison would then suffer from any differences in entrance channel distortions and/or kinematics included in $M_{dsd}(j)$. Nevertheless, a comparison of the case (ii) reactions at the same gamma energy as discussed below reveals that again the two cross sections are of similar magnitude.

To illustrate the effect of the kinematic differences, we can extract from the cross section data the expected E_γ^3 ($L=1$) kinematic factor for the exit gamma channel and compare the thus-modified cross sections at the same proton energy. The modified cross sections are shown in Fig. 6. The solid parallel lines in Fig. 6 are drawn as a guide to the eye to show the approximate exponential dependence of the two reactions. The lines are drawn parallel to illustrate the degree to which the cross sections have the same energy dependence. The ratio of the two modified cross sections is about 0.4, which shows that the γ kinematic differences have a large effect. If the exit channel kinematic factors are removed from the cross section, the 0.4 ratio of the modified cross sections differs

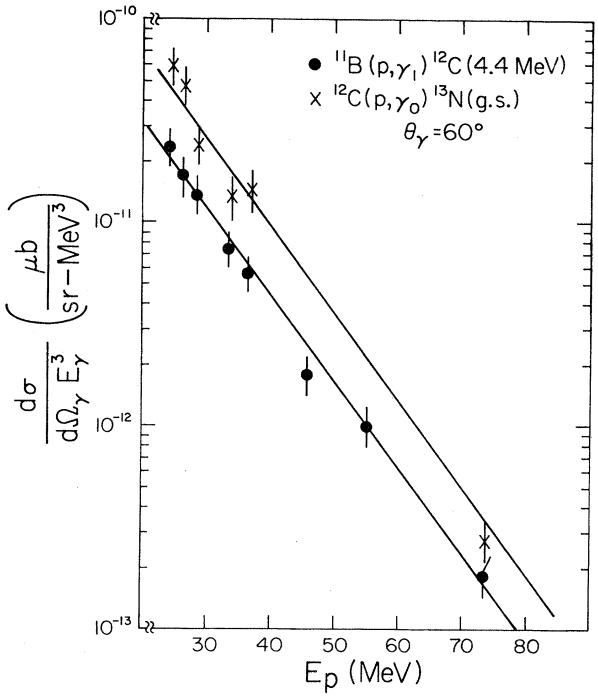

FIG. 6. The energy dependence of the cross section for proton capture into the $p_{1/2}$ orbital in ^{12}C and ^{13}N, with the E_γ^3 energy dependence removed, plotted as a function of center-of-mass proton energy. The solid curves are drawn to show the approximately identical exponential energy dependence of the two reactions.

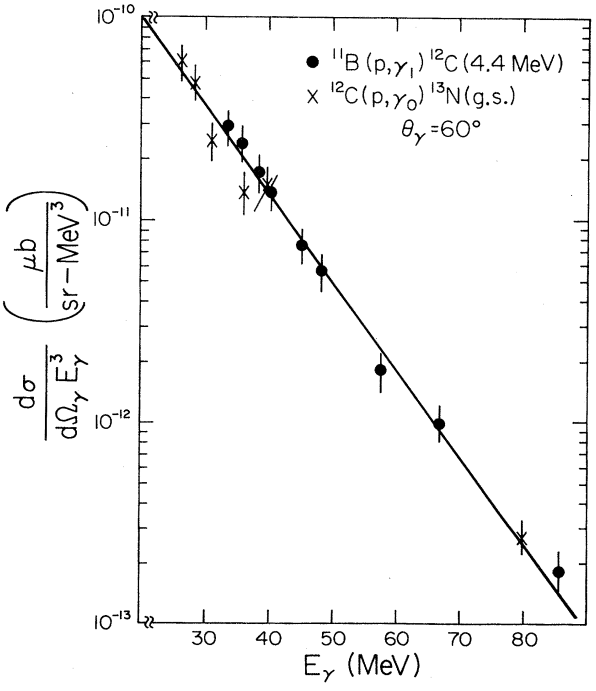

FIG. 7. The same data as in Fig. 6 except plotted as a function of gamma-ray energy for the two reactions.

markedly from the 0.9 value of Eq. (26). [Perhaps the gamma-ray kinematic differences are compensated to some extent by dynamic differences. However, Eq. (26) does not, of course, have the kinematic factors as explicit multipliers, so quantitative comparisons here may not be appropriate.] Finally, in Fig. 7 we show the modified cross sections plotted as a function of gamma energy. Here the ratio of the two cross sections is close to unity (as would be the case for the unmodified cross sections as noted above, since here the factor E_γ^3 removed from each cross section is the same). A striking feature of this plot is the identical, exponential decrease of the modified cross section over the 60 MeV range of gamma energies. A similar energy dependence may also be present in the case (i) reactions above the resonance region, but the paucity of data in this region prevents a more definite conclusion at this time.

V. CONCLUSIONS

We have shown that, for the reaction pair $^{11}B(p,\gamma)^{12}C$ and $^{12}C(p,\gamma)^{13}N$, there is a remarkable similarity in angular distribution and analyzing power data for captures corresponding to the same single-particle transitions in the closed-shell nucleus (1p-1h excitations) and the closed-shell-plus-one-proton nucleus (1p excitations). Further, the ratios of cross sections for corresponding transitions in the two nuclei are related in a simple fashion depending primarily on the single-particle strengths of the states involved, as expressed in their spectroscopic factors. These observations are consistent with a simple direct capture picture of the reactions, but the magnitudes of the cross sections and the constancy of the cross section ratios over a wide energy range, including regions where resonant processes are present, are not compatible with the direct model. Such observations led us to develop the generalized reaction picture presented here, which retains many of the direct-capture model's features while being less restrictive in the necessary assumptions. The new model is insensitive to detailed changes in nuclear structure for proton radiative capture in adjacent closed-shell and closed-shell-plus-one-proton nuclei. In particular, for capture to states in closed shell nuclei the transition is dominated by a single j transfer which can be identified as the j value of the captured particle inferred from the direct capture model. These features are sufficient to account for the equality of both angular distributions and analyzing powers for the transitions compared, as well as for the constancy and magnitude of the ratio of the cross sections over the 60 MeV energy range considered.

Methodology developed here bypasses the question of precise reaction mechanism and the resulting dynamical energy dependence of the transition matrix elements, which determine the absolute magnitude of the cross section and its energy dependence. Since the generalized picture does allow descriptions of some types of transitions not considered in the conventional direct-semidirect models (such as to final states built on 1p-1h excitations of the target's low-lying excited states), studies of capture reactions to specific states for which the simple direct and semidirect transitions are expected to be weak would be highly desirable. For the cases studied in the present work, we have shown that, even with the less-restrictive assumptions of our generalized reaction picture, relations between the capture reaction cross section, angular distribution, and analyzing power data can be nicely understood.

This work was supported in part by The National Science Foundation.

*Present address: MTA KFKI RMKI, Budapest, Hungary.
†Present address: University of Kentucky, Lexington, KY 40506.

[1]M. A. Kovash, S. L. Blatt, R. N. Boyd, T. R. Donoghue, H. J. Hausman, and A. D. Bacher, Phys. Rev. Lett. **42**, 700 (1979).
[2]L. G. Arnold, Phys. Rev. Lett. **42**, 1253 (1979).
[3]S.-F. Tsai and J. T. Londergan, Phys. Rev. Lett. **43**, 576 (1979).
[4]Dean Halderson and R. J. Philpott, Phys. Rev. Lett. **46**, 100 (1981); R. J. Philpott and Dean Halderson, Nucl. Phys. **A375**, 169 (1982).
[5]S. L. Blatt, Los Alamos National Laboratory Report LA-8303-C, 1980, p. 90.
[6]S. L. Blatt, M. A. Kovash, H. J. Hausman, T. R. Donoghue, R. N. Boyd, A. D. Bacher, and C. C. Foster, in *Giant Multipole Resonances,* edited by F. E. Bertrand (Harwood, Chur, Switzerland, 1980), p. 435.
[7]H. R. Weller, H. Hasan, S. Manglos, G. Mitev, N. R. Roberson, S. L. Blatt, H. J. Hausman, R. G. Seyler, R. N. Boyd, T. R. Donoghue, M. A. Kovash, A. D. Bacher, and C. C. Foster, Phys. Rev. C **25**, 2921 (1982).
[8]J. T. Londergan and L. D. Ludeking, Phys. Rev. C **25**, 1722 (1982).
[9]M. Anghinolfi, P. Corvisiero, M. Gauarnone, G. Ricco, M. Sanzone, M. Taiuti, and A. Zucchiatti, in Proceedings of the International Workshop "Medium Energy Interactions in Nuclear Physics," Pavia, 1982 (unpublished).
[10]D. H. Dowell, K. A. Snover, G. Feldman, A. Sandorfi, and M. Collins, Bull. Am. Phys. Soc. **27**, 731 (1982).
[11]P. S. Fisher, D. F. Measday, F. A. Nikolaev, A. Kalmykov, and A. B. Clegg, Nucl. Phys. **45**, 113 (1963).
[12]S. L. Blatt, M. A. Kovash, T. R. Donoghue, R. N. Boyd, H. J. Hausman, and A. D. Bacher, Bull. Am. Phys. Soc. **24**, 843 (1979).
[13]M. A. Kovash, Ph.D. thesis, Ohio State University, 1978; S. L. Blatt and M. A. Kovash (unpublished).
[14]M. A. Kovash and S. L. Blatt, Nucl. Instrum. Methods **163**, 113 (1979).
[15]C. Fred Moore, W. Cottingame, Kenneth G. Boyer, L. E. Smith, Carol Harvey, W. J. Braithwaithe, Christopher L. Morris, H. A. Thiessen, J. F. Amann, M. Devereux, G. Blanpied, G. Burleson, A. W. Obst, S. Iverson, K. K. Seth, R. L. Boudrie, and R. J. Peterson, Phys. Lett. **80B**, 38 (1978); C. L. Morris, J. Piffaretti, H. A. Thiessen, W. B. Cottingame, W. J. Braithwaite, R. J. Joseph, I. B. Moore, D. B. Holtkamp, C. J. Harvey, S. J. Greene, C. F. Moore, R. L. Boudrie, and R. J. Peterson, *ibid.* **86B**, 31 (1979).
[16]N. G. Shevchensko, A. Yu. Buki, B. V. Mazan'ko, V. N. Polishchuk, and A. A. Khomich, Yad. Fiz. **28**, 12 (1978) [Sov. J.

Nucl. Phys. **28**, 5 (1978)].
[17]M. Potakar, Phys. Lett. **92B**, 1 (1980).
[18]C. Mahaux and H. A. Weidenmüller, *Shell Model Approach to Nuclear Reactions* (North-Holland, Amsterdam, 1969), Chap. 3.
[19]G. E. Brown, Nucl. Phys. **57**, 339 (1964).
[20]D. M. Brink, D. Phil. thesis, Oxford University, 1955 (unpublished).
[21]S. Cotanch, Phys. Lett. **76B**, 19 (1978).
[22]R. J. Peterson and J. J. Hamill, Phys. Rev. C **22**, 2282 (1980).
[23]T. W. Donnelly and G. E. Walker, Ann. Phys. (N.Y.) **60**, 209 (1970).
[24]S. S. Hanna, W. Feldman, M. Suffert, and D. Kurath, Phys. Rev. C **25**, 1179 (1982).
[25]S. L. Blatt, T. R. Donoghue, M. A. Kovash, R. N. Boyd, H. J. Hausman, A. D. Bacher, and C. C. Foster, Bull. Am. Phys. Soc. **25**, 603 (1980).
[26]E. G. Adelburger, R. E. Marrs, K. A. Snover, and J. G. Bussoletti, Phys. Rev. C **15**, 484 (1977).
[27]S. Cohen and D. Kurath, Nucl. Phys. **A101**, 1 (1967).